

# Deep phenotyping of the *Cdhr1*<sup>-/-</sup> mouse validates its use in pre-clinical studies for human *CDHR1*-associated retinal degeneration

Imran H. Yusuf, MRCP, FRCOphth,<sup>1,2</sup> Michelle E. McClements, PhD,<sup>1,2</sup> Robert E. MacLaren, FRCOphth, DPhil,<sup>1,2</sup> Peter Charbel Issa, FEBO, DPhil<sup>1,2</sup> \*

<sup>1</sup> Nuffield Laboratory of Ophthalmology, Department of Clinical Neurosciences, Oxford University, West Wing, John Radcliffe Hospital, Oxford, OX3 9DU, UK

<sup>2</sup> Oxford Eye Hospital, John Radcliffe Hospital, Oxford University Hospitals NHS Foundation Trust, Headley Way, Oxford, OX3 9DU, UK

Financial support: National Institute for Health Research (NIHR) Oxford Biomedical Research Centre (BRC), NIHR Senior Investigator Award, Medical Research Council UK (MR/R000735/1)

Conflicts of interest: none

\* Corresponding author

Oxford Eye Hospital, John Radcliffe Hospital

Oxford OX3 9DU

United Kingdom

Telephone: +44 1865 234 737

E-mail: [peter\\_issa@gmx.de](mailto:peter_issa@gmx.de)

Word count (5,000): 3,722

Abstract (500): 250

**Abstract**

**Purpose:** To validate the *Cdhr1*<sup>-/-</sup> mouse as a model for human *CDHR1*-associated retinal degeneration, which may present as cone-rod dystrophy or geographic atrophy.

**Methods:** Deep phenotyping of *Cdhr1*<sup>-/-</sup> (*n*=56) and *C57BL6J* wildtype control mice (*n*=45) was undertaken using *in vivo* multimodal retinal imaging and dark- and light-adapted electroretinography (ERG) over 15 months to evaluate rod- and cone-photoreceptor responses and retinal morphology.

**Results:** *Cdhr1*<sup>-/-</sup> retinas exhibited outer retinal thinning on optical coherence tomography (OCT) at 1-month versus *C57BL6J* (mean 14.6% reduction; *P*<0.0001), with progressive degeneration to 15 months. The OCT layer representing photoreceptor outer segments was more significantly shortened in *Cdhr1*<sup>-/-</sup> eyes at 1 month (mean 33.7% reduction; *P*<0.0001), remained stable to 3 months and was not identifiable at later timepoints. Outer retinal thinning was more pronounced at inferior versus superior retinal locations in *Cdhr1*<sup>-/-</sup> eyes (*P*<0.002 at 3-9 months). Dark-adapted ERG identified severe functional deficits in *Cdhr1*<sup>-/-</sup> mice at 1 month of age versus *C57BL6J* (mean 62% reduction) that continued to decline to 15 months (*P*<0.0001). Light-adapted flicker identified severe deficits in cone function at 1 month (mean 70% reduction), with improved function to 3 months followed by progressive decline (*P*<0.0001).

**Conclusions:** The *Cdhr1*<sup>-/-</sup> mouse exhibits structural and functional evidence of progressive outer retinal degeneration at a slow rate. Early functional deficits affecting both rod and cone photoreceptors in the context of relatively mild structural changes

reflect the human phenotype. This study validates the use of the *Cdhr1*<sup>-/-</sup> mouse for the pre-clinical evaluation of therapeutics for human *CDHR1*-associated retinal degeneration.

### **Key words**

CDHR1; cadherin-related family member 1; cone-rod dystrophy; retinitis pigmentosa; macular dystrophy; macular degeneration; optical coherence tomography; electroretinography; light toxicity

## 1. Introduction

*CDHR1*-associated retinal degeneration is currently an untreatable cause of blindness in humans (OMIM: 609502). (Hanany et al., 2020, Ostergaard et al., 2010, Henderson et al., 2010) Individuals with biallelic truncating variants in *CDHR1* develop progressive cone and rod photoreceptor degeneration manifesting clinically as cone-rod dystrophy, rod-cone dystrophy (retinitis pigmentosa), and individuals with hypomorphic variants manifest late-onset macular dystrophy. (Ba-Abbad et al., 2013, Bessette et al., 2017, Henderson et al., 2010, Ostergaard et al., 2010, Stingl et al., 2017, Duncan et al., 2012, Charbel Issa et al., 2019, Ba-Abbad et al., 2020, Yusuf et al., 2020) Optical coherence tomography imaging in individuals with biallelic truncating variants in *CDHR1* is characterised by progressive outer nuclear layer thinning. (Ba-Abbad et al., 2013, Nikopoulos et al., 2015, Bessette et al., 2017, Stingl et al., 2017) Full-field electroretinography is characterised by more severe, generalised functional defects in both rod and cone photoreceptors than is suggested by retinal imaging studies. (Ba-Abbad et al., 2013)

*CDHR1* encodes a photoreceptor-specific, non-classical cadherin which was identified in 2001 from retinal cDNA libraries. The encoded protein is expressed at the base of the rod and cone photoreceptor outer segments (Rattner et al., 2001) where *CDHR1*-based contacts between developing, nascent outer segment discs and the periciliary ridge of the inner segment appear critical for outer segment disc elongation and morphogenesis. (Burgoyne et al., 2015, Carr et al., 2021) Targeted disruption of the murine homolog, *Cdhr1*, was shown to result in disorganised outer segments on electron microscopy with rod and cone photoreceptor cell death broadly mimicking the

cone-rod dystrophy seen clinically.(Rattner et al., 2001) Electroretinography, undertaken at a single timepoint, identified a reduction in the amplitude of rod and cone responses in *Cdhr1*<sup>-/-</sup> mice compared to *Cdhr1*<sup>+/-</sup> and *Cdhr1*<sup>+/+</sup>.(Rattner et al., 2001)

*CDHR1*-associated retinopathy is an attractive candidate disease for therapeutic gene supplementation and gene editing strategies. A key step towards this aim is the longitudinal characterisation of the *Cdhr1*<sup>-/-</sup> mouse model using *in vivo* techniques. This may both validate the mouse model in the investigation of the human disease, and inform the design of future pre-clinical and clinical studies. In this study, we undertake longitudinal deep phenotyping of the *Cdhr1*<sup>-/-</sup> mouse model using multimodal retinal imaging and electroretinography.

## 2. Materials and Methods

### 2.1 - Animal handling and ethics statement

Animal handling was performed in accordance with the UK Home Office regulations and the ARVO Statement for the Use of Animals in Ophthalmic and Vision Research. Animals were maintained on a 12-hour dark-light cycle with food and water provided *ad libitum*, according to the regulations of the animal care facilities at the University of Oxford. All procedures were evaluated and approved by the Animal Research Ethics Committee of the University of Oxford, under the Home Office Project Licence.

### 2.2 - Animal strains and breeding

*B6;129-Cdhr1<sup>tm1Nat</sup>/J* and *C57BL/6J* mice were obtained from Jackson laboratories (Jackson Laboratory, Bar Harbor, ME, USA). *B6;129-Cdhr1<sup>tm1Nat</sup>/J* mice were originally generated through the targeted disruption of exons 10-17 of the murine *Cdhr1* gene.(Rattner et al., 2001) *B6;129-Cdhr1<sup>tm1Nat</sup>/J* mice were backcrossed to the *C57BL/6J* for 6 generations to achieve a theoretical 98.38% homology to the background strain. The backcross was undertaken to reduce any influence of the background strain on structural or electrophysiological parameters. Separate cohorts of aged mice were used for each timepoint with electroretinography undertaken one week before retinal imaging studies. Data from the right eye of each animal was used for analysis.

### 2.3 - Genotyping of *Cdhr1*<sup>-/-</sup> mutant mice by PCR

The original genotyping primers provided by Jackson Laboratory were unable to distinguish *Cdhr1*<sup>+/-</sup> from *Cdhr1*<sup>-/-</sup> mice; an amplicon was identifiable on polymerase chain reaction (PCR) using wildtype primers with *Cdhr1*<sup>-/-</sup> DNA. This was most probably due to an unintended duplication within the targeted region that had reinserted elsewhere in the genome (personal correspondence with Amir Rattner, PhD, Johns Hopkins). A new wildtype primer set was designed that exploited a single nucleotide polymorphism in the *C57BL/6J* genome (NCBI Gene ID:170677), accurately genotyped *Cdhr1* mice on a *C57BL/6J* background (developed in collaboration with John Hunyara, Johns Hopkins, Baltimore). Primer sequences are provided in **Table A.1**, illustrated against the *C57BL6J Cdhr1* DNA sequence with a comparison of amplicons from primer pairs in **Figure A.1**. DNA was extracted from mouse ear notches by alkaline lysis and PCR amplified using ImmoMix (Bioline Reagent Ltd, UK). PCR cycling conditions were as follows: 95°C for 3 mins; 35 cycles of [95°C for 30

seconds, 62°C for 30 seconds, and 72°C for 30 seconds], 1 cycle of 72°C for 10 mins, 4°C hold.

#### 2.4 - Immunohistochemistry on mouse retina cryosections

Tissue was recovered following schedule 1 sacrifice and enucleation. The cornea was excised at the limbus and lens was removed in 4% paraformaldehyde (Thermo Fisher Scientific). Eye cups were further incubated in 4% paraformaldehyde for 30 mins, before sequential dehydration in 10%, 20% and 30% sucrose. Eye cups were embedded in Optimum Cutting Temperature media (VWR, Radnor, PA, USA) and stored at -80°C prior to sectioning. Cryosectioning of eye cups was undertaken at -20°C in the sagittal plane using 18µm sections (Cryotome LSE; Thermo Fisher Scientific). Slides were permeabilised using 0.2% Triton-X 100, blocked in 10% normal donkey serum (Sigma), and incubated at 4°C overnight in anti-CDHR1 primary antibody. Alex-fluor secondary antibodies (Thermo Fisher Scientific; 488nm or 568nm) were applied at a concentration of 1:500 for 2 hours. Coverslips were mounted using ProLong Diamond anti-fade mountant with DAPI (Thermo Fisher Scientific) to stain nuclear DNA. All slides were imaged using the Leica confocal microscope (Leica Microsystems GmbH, Wetzlar, Germany). Three anti-CDHR1 primary antibodies were used (**Table S2**).

#### 2.5 - Western blot Immunodetection

Four aged-matched mice (one *Cdhr1*<sup>+/+</sup>, one *Cdhr1*<sup>+/-</sup> and two *Cdhr1*<sup>-/-</sup>) all 8-9 weeks post-natal age underwent retinal phenotyping under non-recovery terminal anaesthesia before tissue recovery. Retinae were harvested in cold PBS, placed in 40µl of RIPA buffer (Sigma) with protease inhibitor (Roche) and frozen on dry ice.

Lysates of HEK293T cells were used as the negative control sample. Retinal lysates were homogenised on ice and supernatant removed following centrifugation at 10,000g at 4°C for 20 mins. Protein quantification was achieved using the Quickstart™ Bradford Dye Kit. 30µg of protein was loaded into each lane of a 10% Mini-Protean® TGX™ pre-cast Tris-glycine gel (BioRad) Samples were run at 100V for 1-2 hours. Proteins were transferred to a LF-PVDF membrane. Abcam and Sigma-Aldrich primary antibodies were unsuccessful at detecting CDHR1 in wildtype retinal lysates at a concentration of 1:500. The anti-CDHR1 primary antibody against the c-terminus was used at a concentration of 1:500. Housekeeping primary antibody anti-mouse GAPDH (Origene) was used at a concentration of 1:2,000. Secondary antibodies linked to fluorophores were used at a concentration of 1:10,000; donkey anti-rabbit (800cW) (against anti-CDHR1 primary antibody) and donkey anti-mouse (680cW) (against anti-GAPDH primary antibody).

## 2.6 - Retinal imaging

Retinal imaging studies were conducted as previously described(Charbel Issa et al., 2012) under general anaesthesia, achieved using 80mg/kg of ketamine (Narketan) and 10mg/kg of xylazine (Rompun) administered by intraperitoneal injection. Pupil dilatation was achieved using topical 2.5% Phenylephrine and 1% Tropicamide (Bausch & Lomb, UK) applied to both eyes. Retinal imaging included short-wavelength and near-infrared fundus autofluorescence imaging using 488 and 790 nm excitation light, respectively, and spectral-domain optical coherence tomography imaging with simultaneous recording of a near-infrared (820nm) reflectance image (Spectralis HRA; Heidelberg Engineering, Heidelberg, Germany). Hypromellose 0.5% was used to couple a custom-made contact lens to the cornea.



Optical coherence tomography was undertaken using 4 full-length radial scans centred on the optic disc using high-resolution (HR) mode, averaging 60 B-scans using Automated Real Time (ART) tracking to reduce the effect of movement artefacts. Inner retinal (outer plexiform layer to the internal limiting membrane) and two measurements of outer retinal thickness were recorded: photoreceptor layer thickness (outer plexiform layer to the interdigitation zone) and ellipsoid zone to RPE to capture photoreceptor outer segments. All retinal thickness measurements were taken at 8 identical mid-peripheral retinal loci in each mouse using the callipers on the Heidelberg Spectralis imaging software (**Figure A.2**).

## 2.7 - Electrophysiology

Electrophysiology was undertaken as previously described.(Orlans et al., 2019) The ERG test protocol is detailed in full in **Table A.3**. Briefly, a dark-adapted stimulus-response luminance series progressed through a series of single flashes from an initial stimulus intensity of 10<sup>-6</sup> cd.s/m<sup>2</sup> in log unit increments to a maximum of 25 cd.s/m<sup>2</sup> with a variable number of averaged responses and variable inter-stimulus interval. A dark-adapted 20Hz flicker response was examined thereafter. Four light-adapted steps followed exposure to a rod-saturating full-field 30 cd.s/m<sup>2</sup> white background illumination for 10 minutes. Each of the light-adapted steps were applied on top of this background. An average of 20 responses were average in two light-adapted single-flash assessments followed by 20Hz flicker responses were sequentially assessed at both 3 cd.s/m<sup>2</sup> and 10 cd.s/m<sup>2</sup>.

ERG a- and b-wave amplitudes were measured using Espion v6.0 (Diagnosys LLC). Technically poor replicates were excluded, and trials within the same step were averaged. A-waves amplitudes were measured from the baseline to the trough of the initial negative deflection and B-wave amplitudes were measured from the trough of the A-wave where present, or from the amplitude at stimulus onset when absent, to the peak of the B-wave following the oscillatory potentials. All A-wave and B-wave markers were inspected and adjusted manually where automated designations were inaccurate.

## 2.8 - Statistical analysis

Statistical analysis was performed GraphPad Prism (v9.0.0). All datasets were assessed for normality using the Shapiro-Wilk test. For parametric data, unpaired t-test or two-way ANOVA was used to compare groups with Sidak's multiple comparison test was used according to the characteristics of the dataset. For non-parametric paired datasets, Wilcoxon matched signed-rank test was used.

## 3. Results

### 3.1 - *Cdhr1* expression is absent in *Cdhr1*<sup>-/-</sup> murine retinas

Immunohistochemistry confirmed expression of *Cdhr1* at the base of the photoreceptor outer segments using three anti-CDHR1 primary antibodies against the c-terminus, n-terminal ectodomains and third extracellular cadherin repeat in *C57BL6J* mice (**Figure A.3**). CDHR1 was not identifiable in *Cdhr1*<sup>-/-</sup> retinas using any primary antibody.

Western blotting identified both full length (~120kDa) and the c-terminal fragment (~25kDa) of murine *Cdhr1* in wildtype mice, and identical bands of reduced intensity in *Cdhr1*<sup>+/-</sup> using a primary antibody against the c-terminus. Both the full-length and c-terminal fragment of *Cdhr1* were absent from *Cdhr1*<sup>-/-</sup> retinae and negative control (**Figure A.3**).

### 3.2 - Morphological alterations on OCT imaging in *Cdhr1*<sup>-/-</sup> mice

OCT imaging identified qualitative and quantitative abnormalities of the outer retina in *Cdhr1*<sup>-/-</sup> mice compared to age-matched wildtype controls (**Figure 1, A.4**). In *Cdhr1*<sup>-/-</sup> mice, the ellipsoid zone was present but attenuated at 1 month, and no longer identifiable at 6 months of age. The layer representing photoreceptor outer segments (OS) was thinned and less distinct on OCT imaging up to 3 months of age and lost by 6 months. The external limiting membrane was identifiable up to the age of 6 months, but not at later time-points (**Figure 1A**). OCT reflectivity profiles highlight differences in outer segment length and intensity between genotype groups (**Figure 1B**).

Outer retinal thickness measurements revealed significant photoreceptor layer thinning in 1-month old *Cdhr1*<sup>-/-</sup> mice versus *C57BL6J* controls (mean 84.4 µm vs 102.6 µm at all retinal locations;  $P < 0.0001$ ). Degeneration of the outer retina was progressive in *Cdhr1*<sup>-/-</sup> mice at all retinal locations:  $P < 0.0001$  for 1-month vs 3-15 month time-points) (**Figure 1C & A.5**). In *C57BL6J* mice, outer retinal thinning was identified at 12 ( $p = 0.0006$ ) and 15 months ( $P < 0.0001$ ) but not at earlier timepoints when compared to baseline measurements at 1 month (**Figure 1C**). Analysis of the distance between ellipsoid zone and RPE (defined in **Figure A.2**) was performed in both genotype groups at 1 to 3-month timepoints before the ellipsoid zone was lost in *Cdhr1*<sup>-/-</sup> mice. *Cdhr1*<sup>-/-</sup> exhibited a significantly reduced distance compared to wildtype (mean 49.0 versus

31.2µm;  $P=0.0001$ , unpaired, two-tailed t-test; **Figure A.6**), which did not change from 1 to 3 months in *Cdhr1*<sup>-/-</sup> mice ( $P>0.05$  for all retinal locations).

There was also a mild degree of inner retinal thinning in both genotype groups that was more pronounced in *Cdhr1*<sup>-/-</sup> mice over 15 months (**Figure 1D & A.5**) ( $P<0.0001$  overall for both groups). Inner retinal thickness measurements did not vary significantly with retinal location in either genotype group. The innermost hyper-reflective line appeared thicker at 1 month in *Cdhr1*<sup>-/-</sup> mice.

Outer retinal degeneration occurred at a greater rate at inferior retinal locations versus superior, at 2 months ( $P=0.034$ ) persisting to 9 months ( $P<0.0002$  at all intervening timepoints) (**Figure 1E, A.7**). In *C57BL6J* mice, there was no difference in outer retinal thickness between superior and inferior retinal locations at the same timepoints (data not shown).

### 3.3 - Fundus autofluorescence imaging

Short-wavelength fundus autofluorescence imaging (SW-AF) revealed generalised punctate autofluorescent dots in *Cdhr1*<sup>-/-</sup> mice from 2 months of age (**Figure 2 & A.4, Table A.4**) which varied in size and location on longitudinal imaging of the same eye. At 6 months of age and at all later timepoints, autofluorescent dots were seen in 100% of *Cdhr1*<sup>-/-</sup> mice. In *C57BL6J* mice, autofluorescent dots were absent to 6 months of age at which time a localised distribution could be identified in 2 of 6 mice. At 12 months, 2 of 6 eyes exhibited localised autofluorescent dots, and one demonstrated a generalised distribution. In *Cdhr1*<sup>-/-</sup> mice, there was no loss of autofluorescence indicating that RPE atrophy did not occur to 15 months. SW-AF revealed constriction of the retinal arterioles by 6 months of age, which progressed to severe, generalised

constriction of major retinal arterioles and venules by 15 months of age in *Cdhr1*<sup>-/-</sup> mice  
(**Figure 1 & A.4**).

### 3.4 - Electrophysiology

In 1 month old *Cdhr1*<sup>-/-</sup> mice, mean dark-adapted rod-specific responses (0.01 cd.s/m<sup>2</sup>), as well as maximum A-wave and B-wave amplitudes (10 cd.s/m<sup>2</sup>) were significantly reduced by 26.7%, 62.7% and 40.7%, respectively, compared to *C57BL6J* mice ( $P<0.0001$ ; **Figure 3, A.8 & A.9**). Responses decreased with ageing; at the age of 15 months, responses were extinguished in *Cdhr1*<sup>-/-</sup> mice and approximately 50% of baseline amplitudes in *C57BL6J* mice.

*Cdhr1*<sup>-/-</sup> mice also exhibited significantly reduced responses overall across light-adapted ERG tests compared to *C57BL6J* mice across all tests in the protocol ( $P<0.0001$ ; **Figure 4, A.10 & A.11**). Responses in *Cdhr1*<sup>-/-</sup> mice increased in amplitude across all cone tests between 1 and 3-months after which responses declined, and were extinguished at 15 months. In *C57BL6J* mice, there was a gradual, continuous decline in cone responses with age, which appeared more pronounced in flicker responses compared to single flash responses (**Figure 4, A.10 & A.11**). Whilst single-flash, light-adapted responses at 10 cd.s/m<sup>2</sup> were significantly different between *Cdhr1*<sup>-/-</sup> and wildtype mice at all timepoints ( $P<0.0001$ ), light-adapted flicker responses were not significantly different at 3 and 6 months between genotype groups.

### 3.5 - In vivo structure-function correlation

In *Cdhr1*<sup>-/-</sup> mice, retinal function as measured by both mixed rod-cone and cone ERG responses were more severely affected than structural measures of outer retinal thickness compared to wildtype. Measurements normalised to wildtype measurements

at 1-month were 0.38 for mixed rod-cone (max. scotopic A-wave), 0.3 for cone (20Hz photopic flicker), compared to 0.85 for outer retinal thickness on OCT imaging (**Figure 4A-C**). The thinning of the outer retina at the earliest time point (1 month) seemed to be explained by the reduced distance between ellipsoid zone and RPE (see above), which remained stable from 1-3 months (**Figure 4D & A.6**) whereas subsequent thinning was mainly due to thinning of the outer nuclear layer.

#### 4. Discussion

Longitudinal deep phenotyping of the *Cdhr1*<sup>-/-</sup> mutant mouse over 15 months revealed evidence of slowly progressive outer retinal degeneration on OCT imaging and loss of rod and cone function on electroretinography. These findings recapitulate the major structural and functional characteristics of the human phenotype of *CDHR1*-associated retinal degeneration, validating the use of the *Cdhr1*<sup>-/-</sup> mouse model for pre-clinical studies investigating novel treatments, such as *CDHR1* gene therapy. Moreover, these observations may provide insights into the phenotype and natural history of human *CDHR1*-associated retinal degeneration, which is less well characterised.

Large functional deficits at 1-month affecting rod and cone photoreceptors, out of proportion to structural photoreceptor degeneration in *Cdhr1*<sup>-/-</sup> mice, are likely explained by shortened photoreceptor outer segments, already confirmed by electron microscopy (Rattner et al., 2001), associated with reduced availability of opsins (e.g. a 2-fold reduction in rhodopsin) at 1-month. (Rattner et al., 2001) Accordingly, *in vivo* OCT imaging showed that more severe early alterations (33.7% reduction versus wildtype) are observed in layers representing the photoreceptor inner and outer

segments (reduced reflectivity of the ellipsoid zone and thinning of the adjacent layer representing photoreceptor outer segments), compared to layers representing photoreceptor cell bodies at 1-month (14.6% reduction versus wildtype). Moreover, further thinning of photoreceptor outer segments was not observed to 3 months in *Cdhr1*<sup>-/-</sup> mice. The decline in rod and cone photoreceptor function across this interval is likely to result from photoreceptor cell death as determined by photoreceptor layer thinning, which progressed to 15 months. Since outer segments offer only a small contribution to outer retinal thickness measurements, the rate of functional decline logically exceeds structural degeneration. Beyond 6 months, the rates of functional decline affecting rods and cones are closely matched relative to wildtype controls.

Longitudinal outer nuclear layer thinning forms a structural correlate for progressive functional decline at a rate similar to estimates based on the counting of nuclei on histological sections.(Rattner et al., 2001) The rate of retinal degeneration of the *Cdhr1*<sup>-/-</sup> mouse model, based on OCT data, appears comparable to *Prom1*<sup>rd19</sup>, *Rpe65*<sup>rd12</sup> and *Prph2*<sup>rd2</sup> mouse models.(Collin et al., 2020) *Rpe65*<sup>-/-</sup> mice exhibit diminished scotopic photoreceptor responses (<25% of wildtype) at early timepoints, which are nearly extinguished at 6 months.(Caruso et al., 2010).(Tanabu et al., 2019) Cone responses were diminished by ~80% at early timepoint, similar to the *Cdhr1*<sup>-/-</sup> mice although did not improve in the *Rpe65*<sup>rd12</sup> mouse to 3 months.(Li et al., 2011) In the 1-month-old *Prph2*<sup>rd2</sup> mouse, a ~90% reduction in scotopic B-wave amplitudes was demonstrated which further declined over 6 months,(Reuter and Sanyal, 1984) with abolished photopic responses at all timepoints.(Farjo et al., 2006) There are no longitudinal data for the *Prom1*<sup>rd19</sup> mouse. Thus, despite the similar rates of degeneration based on OCT data, the *Cdhr1*<sup>-/-</sup> mouse exhibits milder early functional

deficits on both the rod and cone systems than *Rpe65*<sup>rd12</sup> and *Prph2*<sup>rd2</sup> mouse models.

*Cdhr1* is expressed at the leading edge of nascent outer segment discs opposite the connecting cilium, and through its ectodomains, forms physical connections with the periciliary ridge of the inner segment.(Burgoyne et al., 2015) These connections appear crucial for horizontal disc elongation and outer segment morphogenesis.(Carr et al., 2021) On review of published reports of human *CDHR1*-associated retinal degeneration, reduced ellipsoid zone reflectivity and shortened outer segments are evident on OCT imaging in early disease.(Ba-Abbad et al., 2013) Moreover, progressive outer retinal degeneration is a universal finding on OCT in individuals with *CDHR1*-associated cone-rod dystrophy, although this has not been quantified. Hence, the human retinal phenotype on OCT imaging seems to parallel our observations in *Cdhr1*<sup>-/-</sup> mice.

An unexpected, novel finding on light-adapted electroretinography in *Cdhr1*<sup>-/-</sup> mice was an increase in cone-related ERG responses to 3 months, consistent across all cone ERG assessments. Possible explanations for this observation include altered higher-level processing within the retina (i.e. lateral inhibition affecting light-adaptation or processing of cone signals)(Tuten et al., 2017), a primary effect of null *Cdhr1* variants on cone development, or an upregulation of an unknown factor secondary to rod cell death. S-opsin has been shown to correctly localise in *Cdhr1*<sup>-/-</sup> mice, with rhodopsin and other outer segment proteins; M-opsin was not examined.(Rattner et al., 2001) However, expression of genes relevant to rod and cone development (i.e. *Crx*, *Nrl* etc.) has not been evaluated in *Cdhr1*<sup>-/-</sup> mutants



versus controls. Further studies are required to determine the mechanism behind this observation; in particular, examination of light-adapted flicker responses at lower frequencies (i.e. 5-7Hz) may further clarify the decrease in cone function.

A further novel finding in this study which may have clinical implications is the observation of an increased rate of retinal degeneration in the inferior retina in *Cdhr1*<sup>-/-</sup> mice, suggesting that light toxicity may be a modifier in *CDHR1*-associated retinal degeneration. *Sfrp1*, a regulator of Adam10 which catalyses the cleavage of the *Cdhr1* ectodomain, releasing the connections between nascent discs and the inner segments, has been shown to significantly enhance light toxicity through an unknown, but perhaps related, mechanism.(Cisneros et al., 2020) This hypothesis may be proven by housing *Cdhr1*<sup>-/-</sup> mice in cages which filter short-wavelength light, as shown to be beneficial in a model of RP.(Orlans et al., 2019) The maximal effect size of inferior versus superior retinal thinning in *Cdhr1*<sup>-/-</sup> mice is smaller than seen in the knock-in *Rho*<sup>P23H/+</sup> mouse model (Cohen's *d*: 2.75 versus 7.07).(Orlans et al., 2019) A predominant inferior pattern of retinal degeneration has been shown in some individuals with biallelic null variants in *CDHR1*.(Haque et al., 2019) However, this requires further clinical investigation.

The *CDHR1* coding sequence (cDNA) is 2,580bp, suitable for encoding with the photoreceptor-specific human rhodopsin kinase promoter (GRK1) and necessary *cis*-acting regulatory elements within a recombinant adeno-associated viral (AAV) vector. The *Cdhr1*<sup>-/-</sup> retinal phenotype identified in this study validates it as a suitable model for the pre-clinical development of a candidate therapeutic for this disorder. Current AAV-delivered retinal gene therapy vectors in clinical trials(Cehajic-Kapetanovic et

al., 2020, Russell et al., 2017, Xue et al., 2018) were enabled by the pre-clinical validation of murine disease models – such as RPE65,(Pang et al., 2006) choroideremia(Tolmachova et al., 2006, Tolmachova et al., 2010) and X-linked rod-cone dystrophy due to variants in retinitis pigmentosa GTPase regulator (RPGR) - prior to proof-of-principle pre-clinical studies.(Fischer et al., 2017) The characterisation and validation of the *Cdhr1*<sup>-/-</sup> mouse model represents a key step towards a therapy for *CDHR1*-associated retinal degeneration.

Phenotypic data presented in this study further support *CDHR1* as an attractive candidate for gene therapy. Firstly, a wide therapeutic window exists for intervention given the slow rate of retinal degeneration. Outer retinal structure is relatively well preserved despite significant functional deficits at early time-points. Early intervention through gene therapy may improve retinal function by restoring photoreceptor outer segment length, and increasing the cellular capacity for proteins critical for phototransduction. Regrowth of photoreceptor outer segments on OCT imaging has been shown to be associated with improvements in visual function following intervention in both *CEP290*(Cideciyan et al., 2019) and *RPGR*-associated photoreceptor degeneration,(Cehajic-Kapetanovic et al., 2020) both of which are also associated with shortened photoreceptor outer segments. Accordingly, the three characteristic hallmarks on OCT imaging of progressive outer nuclear layer thinning, attenuation of the ellipsoid zone and photoreceptor outer segments in *Cdhr1*<sup>-/-</sup> mice may be valuable and relevant structural outcome measures in pre-clinical and clinical studies.

## 5. Conclusions

Longitudinal *in vivo* analysis by electroretinography and multimodal retinal imaging techniques identified early, severe functional deficits in rod and cone function in the *Cdhr1*<sup>-/-</sup> mouse. In the context of relatively mild photoreceptor layer thinning at 1-month, severe early functional deficits are likely attributable to congenitally shortened photoreceptor outer segments. Progressive rod and cone dysfunction over 15 months correlated with gradual photoreceptor layer thinning. A role for light toxicity in *Cdhr1*<sup>-/-</sup> retinas is suggested by a greater rate of photoreceptor cell death in the inferior versus superior retina; a finding reported in mice with targeted disruption of a protein involved in the post-transcriptional regulation of *Cdhr1*, *Sfrp1*. The *Cdhr1*<sup>-/-</sup> mouse recapitulates the human phenotype of *CDHR1*-associated cone-rod degeneration, validating its use in pre-clinical investigation. Slow photoreceptor cell death and early rod and cone dysfunction attributed to shortened photoreceptor outer segments suggest a wide therapeutic window for intervention. Furthermore, evaluation of photoreceptor outer segment length, ellipsoid zone intensity may represent meaningful outcome measures in pre-clinical studies.

## Acknowledgement

We thank Dr. Amir Rattner, PhD, Molecular Biology and Genetics, Johns Hopkins, Baltimore for gifting the anti-*Cdhr1* c-terminal antibody used for immunohistochemistry and western blotting in this study. We thank Mr. John Hunyara, Johns Hopkins, Baltimore for his collaboration in the development of a genotyping strategy for the *Cdhr1* strain.

## References

- Ba-Abbad, R., Robson, A. G., Mahroo, O. A., Wright, G., Schiff, E., Duignan, E. S., Michaelides, M., Arno, G. & Webster, A. R., 2020. A clinical study of patients with novel CDHR1 genotypes associated with late-onset macular dystrophy. *Eye (Lond)*. <https://doi.org/10.1038/s41433-020-1045-3>.
- Ba-Abbad, R., Sergouniotis, P. I., Plagnol, V., Robson, A. G., Michaelides, M., Holder, G. E. & Webster, A. R., 2013. Clinical characteristics of early retinal disease due to CDHR1 mutation. *Mol Vis*. 19, 2250-9. <https://doi.org/10.1167/iovs.14-15647>.
- Bessette, A. P., DeBenedictis, M. J., Traboulsi, E. I., Stingl, K., Mayer, A. K., Llavona, P., Mulahasanovic, L., Rudolph, G., Jacobson, S. G., Zrenner, E., Kohl, S., Wissinger, B. & Weisschuh, N., 2017. Clinical characteristics of recessive retinal degeneration due to mutations in the CDHR1 gene and a review of the literature CDHR1 mutations in retinal dystrophies. *Ophthalmic Genet*. 7, 1-5. <https://doi.org/10.3390/genes8100283>.
- Burgoyne, T., Meschede, I. P., Burden, J. J., Bailly, M., Seabra, M. C. & Futter, C. E., 2015. Rod disc renewal occurs by evagination of the ciliary plasma membrane that makes cadherin-based contacts with the inner segment. *Proc Natl Acad Sci U S A*. 112, 15922-7. <https://doi.org/10.1016/j.neuron.2016.02.004>.
- Carr, B. J., Stanar, P. & Moritz, O. L., 2021. Distinct roles for prominin-1 and photoreceptor cadherin in outer segment disc morphogenesis in CRISPR-altered *X. laevis*. *J Cell Sci*. 134. <https://doi.org/10.1242/jcs.253906>.
- Caruso, R. C., Aleman, T. S., Cideciyan, A. V., Roman, A. J., Sumaroka, A., Mullins, C. L., Boye, S. L., Hauswirth, W. W. & Jacobson, S. G., 2010. Retinal disease in Rpe65-deficient mice: comparison to human leber congenital amaurosis due to RPE65 mutations. *Invest Ophthalmol Vis Sci*. 51, 5304-13. <https://doi.org/10.1167/iovs.10-5559>.
- Cehajic-Kapetanovic, J., Xue, K., Martinez-Fernandez de la Camara, C., Nanda, A., Davies, A., Wood, L. J., Salvetti, A. P., Fischer, M. D., Aylward, J. W., Barnard, A. R., Jolly, J. K., Luo, E., Lujan, B. J., Ong, T., Girach, A., Black, G. C. M., Gregori, N. Z., Davis, J. L., Rosa, P. R., Lotery, A. J., Lam, B. L., Stanga, P. E. & MacLaren, R. E.,

2020. Initial results from a first-in-human gene therapy trial on X-linked retinitis pigmentosa caused by mutations in RPGR. Nat Med. 26, 354-359. <https://doi.org/10.1038/s41591-020-0763-1>.

Charbel Issa, P., Gliem, M., Yusuf, I. H., Birtel, J., Müller, P. L., Mangold, E., Downes, S. M., MacLaren, R. E., Betz, C. & Bolz, H. J., 2019. A Specific Macula-Predominant Retinal Phenotype Is Associated With the CDHR1 Variant c.783G>A, a Silent Mutation Leading to In-Frame Exon Skipping. Invest Ophthalmol Vis Sci. 60, 3388-3397. <https://doi.org/10.1167/iovs.18-26415>.

Charbel Issa, P., Singh, M. S., Lipinski, D. M., Chong, N. V., Delori, F. C., Barnard, A. R. & MacLaren, R. E., 2012. Optimization of in vivo confocal autofluorescence imaging of the ocular fundus in mice and its application to models of human retinal degeneration. Invest Ophthalmol Vis Sci. 53, 1066-75. <https://doi.org/10.1167/iovs.11-8767>.

Cideciyan, A. V., Jacobson, S. G., Drack, A. V., Ho, A. C., Charng, J., Garafalo, A. V., Roman, A. J., Sumaroka, A., Han, I. C., Hochstedler, M. D., Pfeifer, W. L., Sohn, E. H., Taiel, M., Schwartz, M. R., Biasutto, P., Wit, W., Cheetham, M. E., Adamson, P., Rodman, D. M., Platenburg, G., Tome, M. D., Balikova, I., Nerinckx, F., Zaeytijd, J., Van Cauwenbergh, C., Leroy, B. P. & Russell, S. R., 2019. Effect of an intravitreal antisense oligonucleotide on vision in Leber congenital amaurosis due to a photoreceptor cilium defect. Nat Med. 25, 225-228. <https://doi.org/10.1038/s41591-018-0295-0>.

Cisneros, E., di Marco, F., Rueda-Carrasco, J., Lillo, C., Pereyra, G., Martín-Bermejo, M. J., Vargas, A., Sanchez, R., Sandonís, Á., Esteve, P. & Bovolenta, P., 2020. Sfrp1 deficiency makes retinal photoreceptors prone to degeneration. Sci Rep. 10, 5115. <https://doi.org/10.1038/s41598-020-61970-8>.

Collin, G. B., Gogna, N., Chang, B., Damkham, N., Pinkney, J., Hyde, L. F., Stone, L., Naggert, J. K., Nishina, P. M. & Krebs, M. P., 2020. Mouse Models of Inherited Retinal Degeneration with Photoreceptor Cell Loss. Cells. 9. <https://doi.org/10.3390/cells9040931>.

507 Duncan, J. L., Roorda, A., Navani, M., Vishweswaraiah, S., Syed, R., Soudry, S.,  
 508 Ratnam, K., Gudiseva, H. V., Lee, P., Gaasterland, T. & Ayyagari, R., 2012.  
 509 Identification of a novel mutation in the CDHR1 gene in a family with recessive retinal  
 510 degeneration. Arch Ophthalmol. 130, 1301-8.  
 511 <https://doi.org/10.1016/j.neuron.2012.09.037>.

512 Farjo, R., Skaggs, J. S., Nagel, B. A., Quiambao, A. B., Nash, Z. A., Fliesler, S. J. &  
 513 Naash, M. I., 2006. Retention of function without normal disc morphogenesis occurs in  
 514 cone but not rod photoreceptors. J Cell Biol. 173, 59-68.  
 515 <https://doi.org/10.1083/jcb.200509036>.

516 Fischer, M. D., McClements, M. E., Martinez-Fernandez de la Camara, C., Bellingrath,  
 517 J. S., Dauletbekov, D., Ramsden, S. C., Hickey, D. G., Barnard, A. R. & MacLaren, R.  
 518 E., 2017. Codon-Optimized RPGR Improves Stability and Efficacy of AAV8 Gene  
 519 Therapy in Two Mouse Models of X-Linked Retinitis Pigmentosa. Mol Ther. 25, 1854-  
 520 1865. <https://doi.org/10.1016/j.ymthe.2017.05.005>.

521 Hanany, M., Rivolta, C. & Sharon, D., 2020. Worldwide carrier frequency and genetic  
 522 prevalence of autosomal recessive inherited retinal diseases. Proc Natl Acad Sci U S  
 523 A. 117, 2710-2716. <https://doi.org/10.1073/pnas.1913179117>.

524 Haque, M. N., Kurata, K., Hosono, K., Ohtsubo, M., Ohishi, K., Sato, M., Minoshima,  
 525 S. & Hotta, Y., 2019. A Japanese family with cone-rod dystrophy of delayed onset  
 526 caused by a compound heterozygous combination of novel CDHR1 frameshift and  
 527 known missense variants. Hum Genome Var. 6, 18. [https://doi.org/10.1038/s41439-](https://doi.org/10.1038/s41439-019-0048-8)  
 528 [019-0048-8](https://doi.org/10.1038/s41439-019-0048-8).

529 Henderson, R. H., Li, Z., Abd El Aziz, M. M., Mackay, D. S., Eljinini, M. A., Zeidan, M.,  
 530 Moore, A. T., Bhattacharya, S. S. & Webster, A. R., 2010. Biallelic mutation of  
 531 protocadherin-21 (PCDH21) causes retinal degeneration in humans. Mol Vis. 16, 46-  
 532 52. <https://doi.org/10.1136/jmg.2009.069120>.

533 Li, X., Li, W., Dai, X., Kong, F., Zheng, Q., Zhou, X., Lü, F., Chang, B., Rohrer, B.,  
 534 Hauswirth, W. W., Qu, J. & Pang, J. J., 2011. Gene therapy rescues cone structure  
 535 and function in the 3-month-old rd12 mouse: a model for midcourse RPE65 leber

- 536 congenital amaurosis. Invest Ophthalmol Vis Sci. 52, 7-15.  
 537 <https://doi.org/10.1167/iovs.10-6138>.
- 538 Nikopoulos, K., Avila-Fernandez, A., Corton, M., Lopez-Molina, M. I., Perez-Carro, R.,  
 539 Bontadelli, L., Di Gioia, S. A., Zurita, O., Garcia-Sandoval, B., Rivolta, C. & Ayuso, C.,  
 540 2015. Identification of two novel mutations in CDHR1 in consanguineous Spanish  
 541 families with autosomal recessive retinal dystrophy. Sci Rep. 5, 13902.  
 542 <https://doi.org/10.1073/pnas.1509285113>.
- 543 Orlans, H. O., Merrill, J., Barnard, A. R., Charbel Issa, P., Peirson, S. N. & MacLaren,  
 544 R. E., 2019. Filtration of Short-Wavelength Light Provides Therapeutic Benefit in  
 545 Retinitis Pigmentosa Caused by a Common Rhodopsin Mutation. Invest Ophthalmol  
 546 Vis Sci. 60, 2733-2742. <https://doi.org/10.1167/iovs.19-26964>.
- 547 Ostergaard, E., Batbayli, M., Duno, M., Vilhelmsen, K. & Rosenberg, T., 2010.  
 548 Mutations in PCDH21 cause autosomal recessive cone-rod dystrophy. J Med Genet.  
 549 47, 665-9. <https://doi.org/10.1001/archophthalmol.2012.1906>.
- 550 Pang, J. J., Chang, B., Kumar, A., Nusinowitz, S., Noorwez, S. M., Li, J., Rani, A.,  
 551 Foster, T. C., Chiodo, V. A., Doyle, T., Li, H., Malhotra, R., Teusner, J. T., McDowell,  
 552 J. H., Min, S. H., Li, Q., Kaushal, S. & Hauswirth, W. W., 2006. Gene therapy restores  
 553 vision-dependent behavior as well as retinal structure and function in a mouse model  
 554 of RPE65 Leber congenital amaurosis. Mol Ther. 13, 565-72.  
 555 <https://doi.org/10.1016/j.ymthe.2005.09.001>.
- 556 Rattner, A., Smallwood, P. M., Williams, J., Cooke, C., Savchenko, A., Lyubarsky, A.,  
 557 Pugh, E. N. & Nathans, J., 2001. A photoreceptor-specific cadherin is essential for the  
 558 structural integrity of the outer segment and for photoreceptor survival. Neuron. 32,  
 559 775-86.
- 560 Reuter, J. H. & Sanyal, S., 1984. Development and degeneration of retina in rds mutant  
 561 mice: the electroretinogram. Neurosci Lett. 48, 231-7. [https://doi.org/10.1016/0304-](https://doi.org/10.1016/0304-3940(84)90024-7)  
 562 [3940\(84\)90024-7](https://doi.org/10.1016/0304-3940(84)90024-7).
- 563 Russell, S., Bennett, J., Wellman, J. A., Chung, D. C., Yu, Z. F., Tillman, A., Wittes, J.,  
 564 Pappas, J., Elci, O., McCague, S., Cross, D., Marshall, K. A., Walshire, J., Kehoe, T.

- 565 L., Reichert, H., Davis, M., Raffini, L., George, L. A., Hudson, F. P., Dingfield, L., Zhu,  
566 X., Haller, J. A., Sohn, E. H., Mahajan, V. B., Pfeifer, W., Weckmann, M., Johnson, C.,  
567 Gewaily, D., Drack, A., Stone, E., Wachtel, K., Simonelli, F., Leroy, B. P., Wright, J. F.,  
568 High, K. A. & Maguire, A. M., 2017. Efficacy and safety of voretigene neparvovec  
569 (AAV2-hRPE65v2) in patients with RPE65-mediated inherited retinal dystrophy: a  
570 randomised, controlled, open-label, phase 3 trial. *Lancet*. 390, 849-860.  
571 [https://doi.org/10.1016/s0140-6736\(17\)31868-8](https://doi.org/10.1016/s0140-6736(17)31868-8).
- 572 Stingl, K., Mayer, A. K., Llavona, P., Mulahasanovic, L., Rudolph, G., Jacobson, S. G.,  
573 Zrenner, E., Kohl, S., Wissinger, B. & Weisschuh, N., 2017. CDHR1 mutations in retinal  
574 dystrophies. *Sci Rep*. 7, 6992. <https://doi.org/10.1038/s41598-017-07117-8>.
- 575 Tanabu, R., Sato, K., Monai, N., Yamauchi, K., Gonome, T., Xie, Y., Takahashi, S.,  
576 Ishiguro, S. I. & Nakazawa, M., 2019. The findings of optical coherence tomography of  
577 retinal degeneration in relation to the morphological and electroretinographic features  
578 in RPE65<sup>-/-</sup> mice. *PLoS One*. 14, e0210439.  
579 <https://doi.org/10.1371/journal.pone.0210439>.
- 580 Tolmachova, T., Anders, R., Abrink, M., Bugeon, L., Dallman, M. J., Futter, C. E.,  
581 Ramalho, J. S., Tonagel, F., Tanimoto, N., Seeliger, M. W., Huxley, C. & Seabra, M.  
582 C., 2006. Independent degeneration of photoreceptors and retinal pigment epithelium  
583 in conditional knockout mouse models of choroideremia. *J Clin Invest*. 116, 386-94.  
584 <https://doi.org/10.1172/jci26617>.
- 585 Tolmachova, T., Wavre-Shapton, S. T., Barnard, A. R., MacLaren, R. E., Futter, C. E.  
586 & Seabra, M. C., 2010. Retinal pigment epithelium defects accelerate photoreceptor  
587 degeneration in cell type-specific knockout mouse models of choroideremia. *Invest*  
588 *Ophthalmol Vis Sci*. 51, 4913-20. <https://doi.org/10.1167/iovs.09-4892>.
- 589 Tuten, W. S., Harmening, W. M., Sabesan, R., Roorda, A. & Sincich, L. C., 2017.  
590 Spatiochromatic Interactions between Individual Cone Photoreceptors in the Human  
591 Retina. *J Neurosci*. 37, 9498-9509. <https://doi.org/10.1523/jneurosci.0529-17.2017>.
- 592 Xue, K., Jolly, J. K., Barnard, A. R., Rudenko, A., Salvetti, A. P., Patrício, M. I.,  
593 Edwards, T. L., Groppe, M., Orlans, H. O., Tolmachova, T., Black, G. C., Webster, A.  
594 R., Lotery, A. J., Holder, G. E., Downes, S. M., Seabra, M. C. & MacLaren, R. E., 2018.



595 Beneficial effects on vision in patients undergoing retinal gene therapy for  
596 choroideremia. Nat Med. 24, 1507-1512. <https://doi.org/10.1038/s41591-018-0185-5>.  
597 Yusuf, I. H., MacLaren, R. E. & Charbel Issa, P., 2020. CDHR1-related late-onset  
598 macular dystrophy: further insights. Eye (Lond). [https://doi.org/10.1038/s41433-020-](https://doi.org/10.1038/s41433-020-01212-3)  
599 [01212-3](https://doi.org/10.1038/s41433-020-01212-3).  
600



**Figure 1. Longitudinal *in vivo* optical coherence tomography retinal imaging characteristics in *Cdhr1*<sup>-/-</sup> mice. (A)** Optical coherence tomography (OCT) retinal imaging studies identified an indistinct ellipsoid zone and photoreceptor outer segment layer in *Cdhr1*<sup>-/-</sup> mice at 1 month; neither are discernible at 6 months. Progressive thinning of the outer retina is seen at 6 and 12 months (additional timepoints shown in Figure S4). Thickening of the innermost hyperreflective band is seen in *Cdhr1*<sup>-/-</sup> mice at 1 month, also shown in panel B. **(B)** OCT reflectivity profiles confirm outer retinal thinning at 1 month in *Cdhr1*<sup>-/-</sup> mice. The EZ reflection is diminished with reduced width and depth of the adjacent OS band, indicated by coloured boxes on the reflectivity profile. At 12 months, the outer retina is thinner and ELM and EZ are absent in *Cdhr1*<sup>-/-</sup> mice. **(C)** Photoreceptor layer thickness measurements on OCT imaging in *Cdhr1*<sup>-/-</sup> mice are reduced at 1 month compared to wildtype controls (mean 100.2µm vs 85.6µm). Data points represent measurements from the superior retina only. Repeated measures two-way ANOVA for overall effect of genotype on photoreceptor layer thickness:  $F_{1,152} = 1754$ ,  $p < 0.0001$ . Progressive outer retinal degeneration is seen in *Cdhr1*<sup>-/-</sup> mice to 15 months ( $p < 0.0001$ , two-way ANOVA). In *C57BL6J* mice, the outer retina is not significantly thinned until 12 months of age ( $p = 0.0006$ ; two-way ANOVA). **(D)** The inner retina is thickened in *Cdhr1*<sup>-/-</sup> mice at 1-month of age compared to wildtype with mild progressive thinning to 15 months. **(E)** Photoreceptor layer thinning progresses more quickly at inferior when compared to superior retinal locations in *Cdhr1*<sup>-/-</sup> mice as shown across 8 retinal loci. Repeated measures two-way ANOVA for overall effect of retinal location on photoreceptor layer thickness in *Cdhr1*<sup>-/-</sup> mice:  $F_{7,408} = 20.17$ ,  $P < 0.0001$ . A direct comparison of superior and inferior retinal thickness measurements across age

groups *Cdhr1*<sup>-/-</sup> cohort identifies significant inferior retinal thinning from 2-9 months ( $p < 0.05$  at all timepoints; two-way ANOVA).

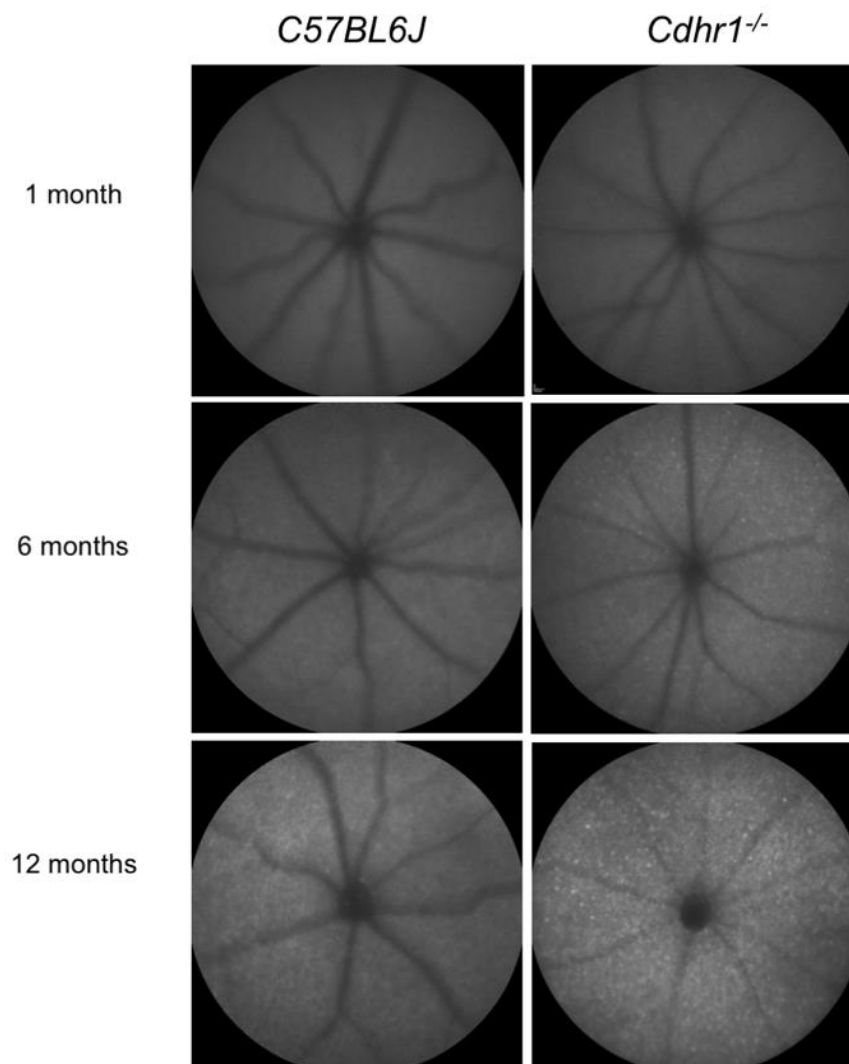


**Figure 2. Short-wavelength fundus autofluorescence (SW-AF) imaging in *Cdhr1*<sup>-/-</sup> mice.** Generalised punctate autofluorescent dots are identifiable in *Cdhr1*<sup>-/-</sup> retinas from 2 to 15 months (additional timepoints shown in Figure S4). Generalised constriction of retinal vessels is seen in *Cdhr1*<sup>-/-</sup> mice after the 6-month timepoint.

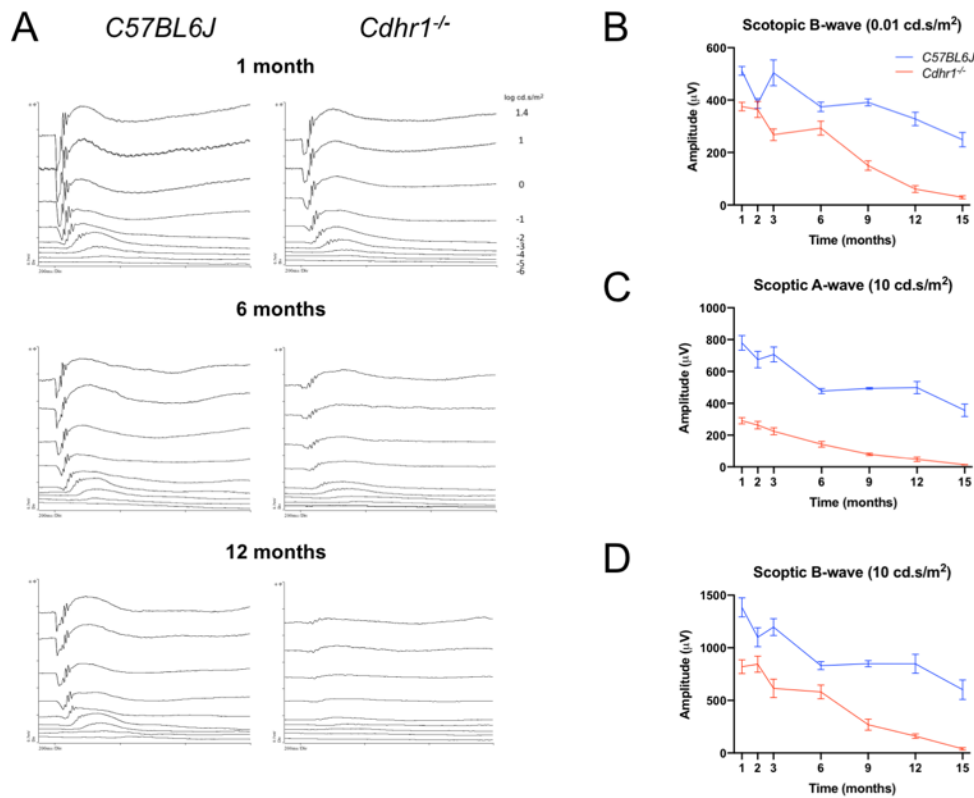


**Figure 3. Functional testing by longitudinal dark-adapted electroretinography**

**in *Cdhr1*<sup>-/-</sup> and *C57BL6J* mice. (A)** Representative raw dark-adapted ERG traces at 1, 6 and 12 months. **(B)** Scotopic B-wave responses at 0.01 cd.s/m<sup>2</sup> were significantly reduced in *Cdhr1*<sup>-/-</sup> mice. Repeated measures two-way ANOVA for overall effect of genotype  $F_{1,91} = 182.7$ ,  $P < 0.0001$ . Responses did not differ significantly at 2- and 6- month timepoints. **(C)** Scotopic A-wave responses at 10 cd.s/m<sup>2</sup> were significantly reduced in *Cdhr1*<sup>-/-</sup> mice ( $p < 0.0001$  for all timepoints). Repeated measures two-way ANOVA for overall effect of genotype on A-wave amplitude:  $F_{1,92} = 554.8$ ,  $P < 0.0001$ . **(D)** Scotopic B-wave responses at 10 cd.s/m<sup>2</sup> were significantly reduced in *Cdhr1*<sup>-/-</sup> mice ( $P < 0.0001$ , except at 2- and 6- months). Repeated measures two-way ANOVA for overall effect of genotype on B-wave amplitude:  $F_{1,92} = 136.6$ ,  $P < 0.0001$ . Mean and SEM across representative flash intensities are presented, with full datasets presented in Figure S8 & S9.

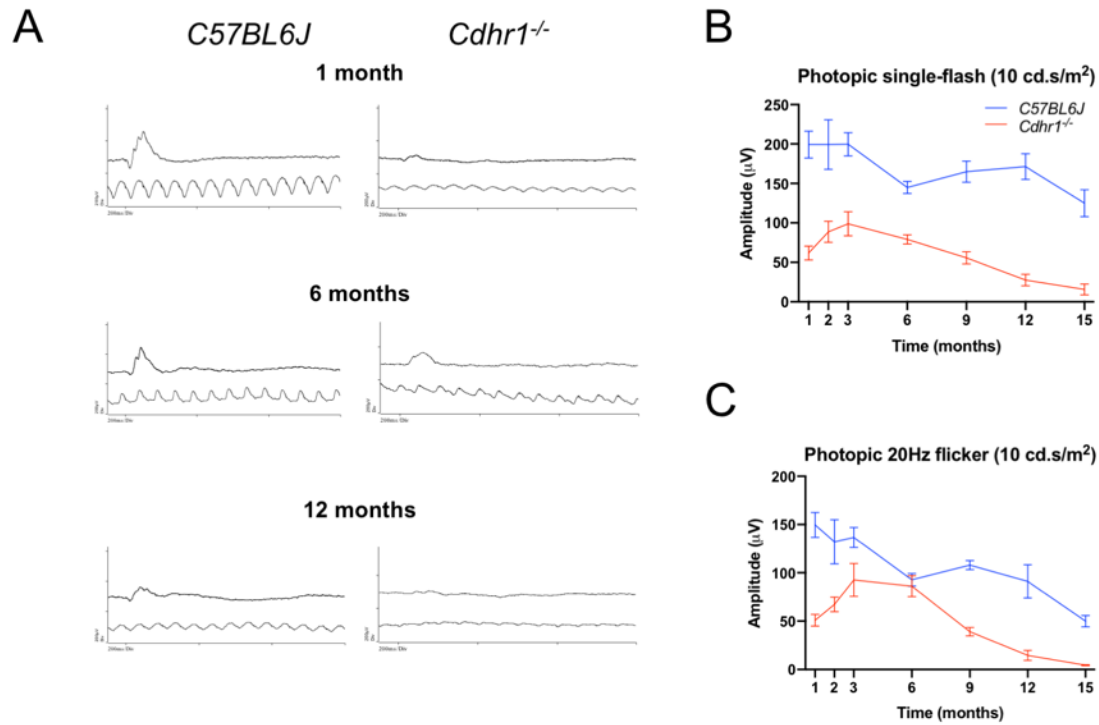


**Figure 4. Functional testing by longitudinal light-adapted electroretinography in *Cdhr1*<sup>-/-</sup> and C57BL6J mice.** (A) Representative raw ERG traces at 1, 6 and 12 months showing single-flash (above) and 20Hz flicker responses (below) at 10 cd.s/m<sup>2</sup> (B) Photopic single-flash response responses were significantly reduced in *Cdhr1*<sup>-/-</sup> mice ( $P < 0.05$  for all timepoints). Repeated measures two-way ANOVA for overall effect of genotype on photopic single-flash amplitude:  $F_{1,92} = 182.8$ ,  $p < 0.0001$ . (C) Photopic 20Hz flicker responses were significantly reduced overall in *Cdhr1*<sup>-/-</sup> mice. Repeated measures two-way ANOVA for overall effect of genotype on photopic flicker responses:  $F_{1,92} = 89.42$ ,  $P < 0.0001$ . However, responses did not differ by genotype at the 3- and 6-month timepoints on Šidák's multiple comparisons test at both flash intensities. Mean and SEM across representative flash intensities are presented, with full datasets presented in Figure S10 & S11.

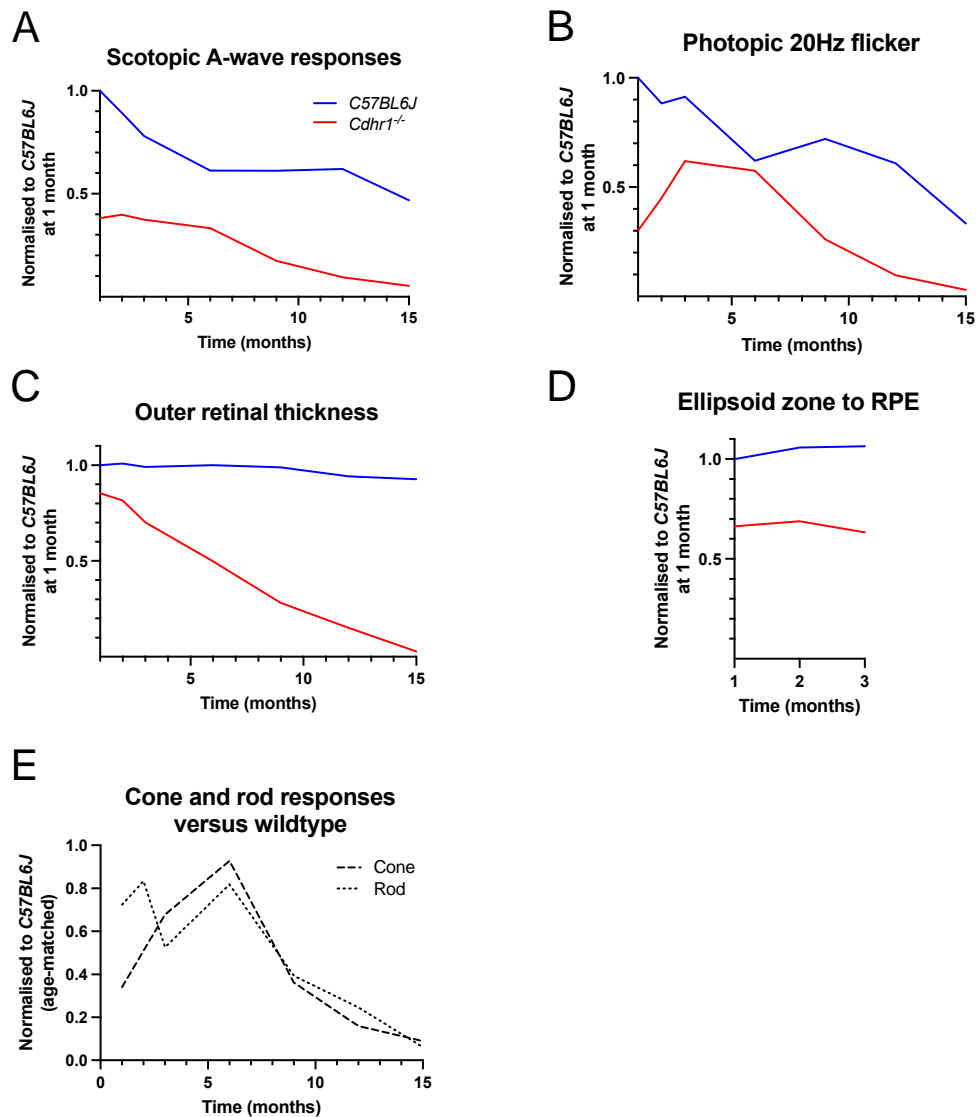


**Figure 5. Relative structural degeneration and functional decline over time in *Cdhr1*<sup>-/-</sup> mice.** (A) Mixed rod-cone (10cd.s/m<sup>2</sup>) A-wave responses on dark-adapted ERG normalised to C57BL6J responses at 1 month shows severe functional deficits at 1-month (62% reduction) when compared to outer retinal thickness measurements on OCT imaging in (C). (B) Normalised light-adapted 20Hz flicker responses exhibited severe deficits in cone function (70% reduction) in *Cdhr1*<sup>-/-</sup> mice at 1 month, with improvement of responses to 3 months, followed by decline. (D) OCT measurements of ellipsoid zone to RPE, normalised to C57BL6J at 1 month shows stable retinal measurements to 3 months. The ellipsoid band is lost in *Cdhr1*<sup>-/-</sup> mice at

674 later timepoints. **(E)** Longitudinal cone (photopic 20Hz flicker at 10.cd/s/m<sup>2</sup>) and rod  
675 (scotopic B-wave responses at 0.1cd/s/m<sup>2</sup>) responses in *Cdhr1*<sup>-/-</sup> mice, normalised to  
676 to age-matched *C57BL6J*, shows progressive increase in cone responses to 3  
677 months followed by decline to 15 months. Rod responses are less affected at 1  
678 month although the rate of functional loss beyond 6 months appears to match that of  
679 cones.



**Table A.1.** Primer sequences used in the genotyping of *Cdhr1*<sup>-/-</sup> mutant mice by polymerase chain reaction.

Primer name	Sequence (5' to 3')	Amplicon size
Wildtype allele forward	ATCTGGTCTGAGAGCCCCCAT	500bp
Wildtype allele reverse	CAAACACAGACTGGGGGCGGTA	
Mutant allele forward	GGAAGGTGCCACTCCCCTGTCC	300bp
Mutant allele reverse	CTTACCTGTTTGTATCGCTACATCC	

**Table A.2.** Anti-CDHR1 primary antibodies

Manufacturer	Antigenic epitope (aa)	Homology	CDHR1 domain	Clonality & Conjugation	Host Species	Concentration
Abcam	50-100	98%	1 <sup>st</sup> & 2 <sup>nd</sup> cadherin repeat	Polyclonal Unconjugated	Chicken	IHC: 1:100
Sigma-Aldrich	250-325	84%	3 <sup>rd</sup> cadherin repeat	Polyclonal Unconjugated	Rabbit	IHC: 1:100
Johns Hopkins* Whole serum	844-858	87%	C-terminus	Polyclonal**	Rabbit	IHC: 1:1000 WB: 1:1000

aa – amino acid; \* - gifted by Nathan's laboratory, Johns Hopkins; \*\* - unpurified whole serum

**Table A.3.** Full-field electroretinography protocol

Step	Flash intensity [cd.s/m <sup>2</sup> ]	Repetitions	Inter-stimulus interval [sec]	Interval after intensity step [sec]	
0	Dark adaptation: Overnight				
1	0.000001	10	5	10	Scotopic testing
2	0.00001	10	5	20	
3	0.0001	10	5	20	
4	0.001	10	5	20	
5	0.01	10	5	20	
6	0.1	5	20	60	
7	1	5	20	60	
8	10	5	20	60	
9	25	5	20	120	
10	3	20 traces	20Hz flicker		
	Pre-exposure: Rod-saturating steady full-field white background illumination (30 cd/m <sup>2</sup> ) for 10 min				
11	3	10	2		Photopic testing
12	3	20 traces	20Hz flicker		
13	10	10	2		
14	10	20 traces	20Hz flicker		

**Table A.4.** Frequency of autofluorescent dots on SW-AF imaging in *Cdhr1*<sup>-/-</sup> and *C57BL6J* mice.

	<b><i>C57BL6J</i></b>	<b><i>Cdhr1</i><sup>-/-</sup></b>
<b>1 month</b>	0% ( <i>n</i> =12)	16% ( <i>n</i> =8)
<b>2 months</b>	0% ( <i>n</i> =6)	80% ( <i>n</i> =10)
<b>3 months</b>	0% ( <i>n</i> =6)	83% ( <i>n</i> =14)
<b>6 months</b>	33% ( <i>n</i> =6) (localised)	100% ( <i>n</i> =8)
<b>9 months</b>	33% ( <i>n</i> =5) (localised)	100% ( <i>n</i> =7)
<b>12 months</b>	66% ( <i>n</i> =6) (2 localised, 1 generalised)	100% ( <i>n</i> =6)
<b>15 months</b>	83% ( <i>n</i> =6) (4 localised, 1 generalised)	100% ( <i>n</i> =6)

Localised – 2 or fewer quadrants; Generalised – 3 or more quadrants